Received: 22 August 2017 | Accepted: 23 January 2018

DOI: 10.1002/hyp.11459

RESEARCH ARTICLE

WILEY

Intercomparison of snow water equivalent observations in the Northern Great Plains

Samuel E. Tuttle[1†] | Jennifer M. Jacobs[1] | Carrie M. Vuyovich[2] | Carrie Olheiser[3] | Eunsang Cho[1]

[1] University of New Hampshire, 105 Main Street, Durham, NH 03824, USA

[2] U.S. Army Corps of Engineers, Cold Regions Research and Engineering Laboratory, 72 Lyme Road, Hanover, NH 03755, USA

[3] National Weather Service Office of Water Prediction—Minnesota, 1735 Lake Drive West, Chanhassen, MN 55317, USA

Correspondence
Samuel E. Tuttle, University of New Hampshire, 105 Main Street, Durham, NH 03824, USA.
Email: stuttle@mtholyoke.edu

Present Address
[†] Samuel E. Tuttle's present address is Mount Holyoke College, 50 College Street, South Hadley, MA 01075, USA.

Funding information
NASA Applied Sciences, Grant/Award Number: NNX15AC47G

Abstract

In the Northern Great Plains, melting snow is a primary driver of spring flooding, but limited knowledge of the magnitude and spatial distribution of snow water equivalent (SWE) hampers flood forecasting. Passive microwave remote sensing has the potential to enhance operational river flow forecasting but is not routinely incorporated in operational flood forecasting. We compare satellite passive microwave estimates from the Advanced Microwave Scanning Radiometer for the Earth Observing System (AMSR-E) to the National Oceanic and Atmospheric Administration Office of Water Prediction (OWP) airborne gamma radiation snow survey and U.S. Army Corps of Engineers (USACE) ground snow survey SWE estimates in the Northern Great Plains from 2002 to 2011. AMSR-E SWE estimates compare favourably with USACE SWE measurements in the low relief, low vegetation study area (mean difference = −3.8 mm, root mean squared difference [RMSD] = 34.7 mm), but less so with OWP airborne gamma SWE estimates (mean difference = −9.5 mm, RMSD = 42.7 mm). An error simulation suggests that up to half of the error in the former comparison is potentially due to subpixel scale SWE variability, limiting the maximum achievable RMSD between ground and satellite SWE to approximately 26–33 mm in the Northern Great Plains. The OWP gamma versus AMSR-E SWE comparison yields larger error than the point-scale USACE versus AMSR-E comparison, despite a larger measurement footprint (5–7 km^2 vs. a few square centimetres, respectively), suggesting that there are unshared errors between the USACE and OWP gamma SWE data.

KEYWORDS

AMSR-E, gamma radiation, Northern Great Plains, passive microwave, remote sensing, snow survey, snow water equivalent, SWE

1 | INTRODUCTION

In the Northern Great Plains, especially the Red River of the North Basin, snowmelt is a dominant driver of flooding (Berghuijs, Woods, Hutton, & Sivapalan, 2016). For example, the record-breaking 1997 Red River spring snowmelt flood damaged 85% of structures in the Grand Forks, North Dakota area and totalled $4 billion in U.S. damages, due to failure of the protective dikes around the city after miscommunication and under-prediction of the flood peak (Pielke, 1999; Todhunter, 2001). The 1997 flood, and additional major snowmelt floods in 2009 and 2011, forced preparations and evacuations, and inundated homes, resulting in large societal and economic impacts to communities in North Dakota and Minnesota in the United States and the Canadian province of Manitoba (Rannie, 2016; Stadnyk, Dow, Wazney, & Blais, 2016; Todhunter, 2001; Wazney & Clark, 2016). Accurate flood forecasts are important to help agencies and communities prepare for flood events and prevent damages, as well as properly allocate flood management efforts and funds. In the north central United States, the National Weather Service (NWS) North Central River Forecast Center (NCRFC) provides spring flood forecasts in order to prepare and/or evacuate at-risk communities. Unfortunately, forecasting of flood levels has proven difficult in the region, partly due to insufficient information about snow properties. For instance, as recently as 2013, with the observational data sets and models that were available at the time, the NCRFC forecasted a peak flow that exceeded the observed by 70%.

The most important measure of snow for water resources applications is snow water equivalent (SWE), which is the depth of liquid water that would result if all snow on the ground surface melted. Currently, SWE in the Northern Great Plains, like many other regions of the country, is measured in situ at ground stations and remotely via aircraft using gamma radiation methods (Carroll, 2001). In situ ground measurements are the most trusted (i.e., accurate) SWE observations, but the spatial footprint of these measurements is very small (on the scale of centimetres) and daily (or even weekly) data are only available in a handful of locations in the region. Additionally, snow properties can vary considerably over small distances, especially in windy or rugged areas (Carroll & Carroll, 1989; Cork & Loijens, 1980), so the "true" SWE value of a large area is often unknown and may not accurately be characterized by a single measurement site (e.g., Clark et al., 2011).

The airborne gamma radiation snow survey (Carroll, 2001; Carroll & Schaake Jr, 1983; Peck, Bissell, Jones, & Burge, 1971; Peck, Carroll, & VanDemark, 1980), currently operated by the National Oceanic and Atmospheric Administration (NOAA) Office of Water Prediction (OWP; and formerly by the National Operational Hydrologic Remote Sensing Center (NOHRSC)), provides SWE observations to regional flood forecasting centres over a network of flight lines with spatial footprints of 5–7 km^2. This larger measurement scale reduces effects from small-scale SWE variability. However, operational limitations restrict the number of observations from each flight line, so SWE data are received from each flight line only four or fewer times per winter.

Satellite passive microwave radiometry (Chang, Gloersen, Schmugge, Wilheit, & Zwally, 1976; Hallikainen, Ulaby, & Abdelrazik, 1986; Mätzler, 1987; Ulaby & Stiles, 1980) can provide another source of SWE information that is not currently used by operational flow forecasting centres in the region. Satellite observations are available on a daily basis at low spatial resolution over the entire region, which could improve the temporal resolution and spatial coverage of SWE data available from current observations. Some of the initial passive microwave SWE studies were conducted in the Northern Great Plains (e.g., Foster et al., 1980), along with continued SWE algorithm development (Foster, Barton, Chang, & Hall, 2001; Gan, Kalinga, & Singh, 2009; Josberger & Mognard, 2002; Josberger, Mognard, Lind, Matthews, & Carroll, 1998; Mognard & Josberger, 2002; Singh & Gan, 2000), which lends confidence to quality of the satellite observations in the region. A handful of studies have evaluated passive microwave estimates in the Northern Great Plains and southern Canadian prairies. Chang et al. (2005) compared in situ ground observations of snow depth to Special Sensor Microwave Imager (SSM/I) satellite snow depth estimates in the Northern Great Plains, indicating that multiple ground observations are necessary in order to approximate the larger scale satellite estimates (see Section 6.2). Mote, Grundstein, Leathers, and Robinson (2003) compared SSM/I SWE to in situ measurements and SWE from the SNTHERM model at five stations in the Northern Great Plains. The authors found that the SSM/I SWE overestimated in situ SWE in late winter, likely due to metamorphism and grain growth.

Operational flood forecasters still struggle to accurately determine how much water equivalent is stored in the snowpack and could potentially contribute to spring snowmelt flooding (Pedro Restrepo and Mike DeWeese, NOAA NCRFC, and personal communications). The long-term vision is to operationalize satellite passive microwave observations to improve snowmelt driven flood forecasting for water management applications (Tuttle et al., 2017). Fulfilling this vision requires evaluation of microwave SWE data with respect to current data sources and, ultimately, identification of an optimal combination of those data sources that maximizes the available knowledge from different measurement techniques. Although passive microwave SWE measurements have strong potential to support water resources management, no previous studies have compared passive microwave SWE to current operational gamma airborne and ground observations for watershed applications. Although past analyses have evaluated passive microwave SWE in the Northern Great Plains, detailed examination of estimates from the Advanced Microwave Scanning Radiometer for the Earth Observing System (AMSR-E) in this area are limited. Similarly, few studies have compared OWP gamma observations to passive microwave estimates (Gan et al., 2009; Mote et al., 2003; Singh & Gan, 2000).

In this analysis, we examine the relationships between satellite SWE and other SWE observations in the Northern Great Plains in order to understand the potential value of passive microwave SWE observations for flood forecasting purposes and to provide a baseline of historical ground and airborne observations available to support for future snow satellite missions. We compare AMSR-E SWE estimates to two independent sources of SWE observations that are currently used to support flood forecasting in the region: (1) U.S. Army Corps of Engineers (USACE) ground snow surveys and (2) NOAA OWP airborne gamma radiation snow surveys (hereafter, "OWP gamma SWE"). The following sections will describe the study area, each of the SWE data sources, and the methods of comparison, followed by presentation and discussion of results.

2 | STUDY AREA

The study region (Figure 1) comprises parts of the north central United States and southern Canadian prairies, an area of approximately 700,000 km^2. This area includes parts of the Mississippi, Missouri, and Assiniboine-Red River drainage basins. The region is generally flat lying with little vegetation cover during winter and dominated by agricultural (65%) and temperate grassland (27%) land cover types (North American Land Change Monitoring System, 2010). Therefore, two aspects that complicate estimation of passive microwave and airborne gamma radiation SWE—dense vegetation and rugged terrain—are largely absent from the study area.

The annual mean air temperature of the study region ranges from 11 °C in the south-eastern part of the region (Iowa) to 1 °C in the north (Canadian prairies), and the annual precipitation decreases from 100 cm in the southeast to 35 cm in the west (western North Dakota; Willmott & Matsuura, 2001, updated 2015). December to April precipitation is between 5 and 10 cm for most of the region, reaching 20 cm in the southeast. A vast majority of the study area (88%) falls under the "prairie" snow classification from Liston and Sturm (2014), which is characterized by shallow (usually <1 m), moderately cold snowpacks that are highly affected by windy conditions (i.e., snow drifts and wind

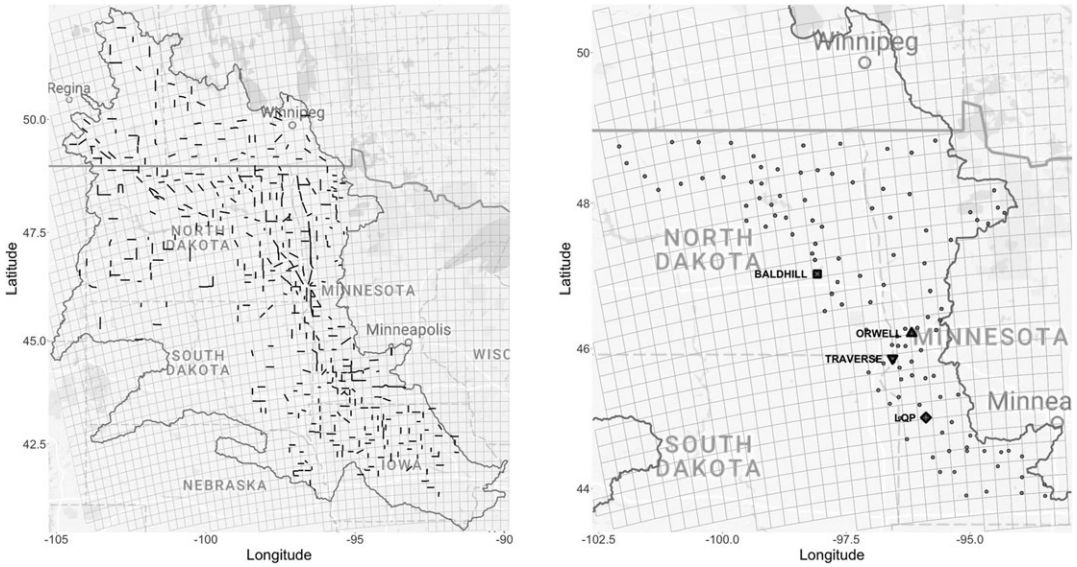

FIGURE 1 Maps showing the locations of observations used in this analysis. The study area, comprising generally low relief, agricultural or prairie areas of the north central United States and southern Canada, is denoted by the dark grey outline. The left panel displays the Advanced Microwave Scanning Radiometer for the Earth Observing System pixel grid (grey boxes) and the Office of Water Prediction gamma snow survey flight lines (black lines) used in this analysis. The right panel shows the subset of the study area for which U.S. Army Corps of Engineers ground snow water equivalent estimates were collected. The Advanced Microwave Scanning Radiometer for the Earth Observing System grid is again shown, along with U.S. Army Corps of Engineers annual survey sites (circles) and weekly survey sites (labelled black polygonal symbols) within the study area

slabs common). Another 8% of the study area is warm forest, along with 1% tundra, 1% taiga, and 2% open water.

3 | DATA

The data used in this analysis are restricted to the time period of the AMSR-E satellite instrument, which operated aboard the polar-orbiting Aqua satellite platform from June 18, 2002, until October 4, 2011. The SWE observations used in this study are detailed in the following sections, including theoretical bases, sampling methodologies, and uncertainties inherent in each data source.

3.1 | AMSR-E passive microwave SWE

Microwave radiation is naturally emitted from the land surface, including soil, snow, and vegetation. Snow crystals scatter and absorb microwave radiation, and deeper snowpacks lead to more scattering and lower brightness temperatures than shallower snowpacks, for a given snow grain size and temperature (Chang et al., 1976; Chang, Foster, Hall, Rango, & Hartline, 1982; Ulaby & Stiles, 1980). Snowpack attenuation is also affected by snow grain size and density (Chang et al., 1976; Josberger & Mognard, 2002; Kelly, Chang, Tsang, & Foster, 2003; Ulaby & Stiles, 1980). Microwave radiation at higher frequencies is scattered more effectively than at lower frequencies, leading to observation of different brightness temperatures in different portions of the microwave spectrum (Chang, Foster, & Hall, 1987; Ulaby & Stiles, 1980). This is the basis for operational SWE algorithms (e.g., Kelly, 2009), which scale the difference between a high-frequency (typically 37 GHz) and low-frequency (typically 18 GHz) brightness temperature measurement by an empirical factor that accounts for an assumed snow density and grain size in order to obtain to SWE. The brightness temperature difference technique is often referred to as the *Chang algorithm* (Chang et al., 1987). Use of the brightness temperature difference minimizes the snow temperature effect on the microwave signal and for frozen or dry underlying soils, limits the effect of subsurface roughness and dielectric properties (Kelly et al., 2003). Updates of the Chang method include corrections for forest fraction and snow grain size (e.g., the operational AMSR-E algorithm; Kelly, 2009). Limitations to passive microwave SWE estimates include poor performance in densely forested areas, in mountainous terrain with deep snowpacks, and in close proximity to large water bodies (Dong, Walker, & Houser, 2005; Hancock, Baxter, Evans, & Huntley, 2013; Vuyovich, Jacobs, & Daly, 2014). Furthermore, passive microwave SWE estimates are not reliable when liquid water is present in the snowpack or on the land surface because the microwave signal no longer has the desired scattering behaviour (Stiles & Ulaby, 1980; Walker & Goodison, 1993). Although atmospheric changes may alter the attenuation of the microwave signal, this error is assumed to be small for SWE frequencies (Tedesco & Narvekar, 2010), but recent findings suggest that this may not be the case for frequencies 37 GHz or higher (Wang & Tedesco, 2007; Tedesco & Wang, 2006; Ronny Schroeder, personal communication). Additionally, spatial interpolation during gridding of the passive microwave brightness temperature data, along with the difference in instantaneous field of view of satellite instruments at different microwave frequencies, may introduce error into passive microwave SWE estimates. Tedesco and Narvekar (2010) provide a summary of the current limitations of operational passive microwave snow estimates.

The passive microwave SWE data used in this study (AE_DySno; Tedesco, Kelly, Foster, & Chang, 2004) derive from the AMSR-E satellite instrument. AMSR-E had near-complete global coverage on a daily basis, with equatorial overpass times of approximately 1:30 a.m. (descending) and 1:30 p.m. (ascending) local time. Only data

from the descending overpass were used to create the AE_DySno SWE product, in order to minimize the impact of wet snow. The AMSR-E SWE algorithm (Kelly, 2009; Chang & Rango, 2000) not only uses the basic framework of the Chang algorithm (i.e., brightness temperature difference between the 36.5 and 18.7 GHz channels; Chang, Foster, & Hall, 1996; Foster, Chang, & Hall, 1997) but also includes higher (89.0 GHz), intermediate (23.8 GHz), and lower (10.7 GHz) frequency microwave observations in order to identify shallow and deep snow, as well as the ratio between horizontal and vertical polarization at the 36.5 and 18.7 frequencies in order to account for snow metamorphism (i.e., grain growth). The daily L3 AMSR-E SWE data are provided at 25-km resolution in Northern Hemisphere Equal-Area Scalable Earth Grid format on the National Snow and Ice Data Center website (https://nsidc.org/data/ae_dysno). The AMSR-E grid is shown in grey in Figure 1.

3.2 | USACE ground snow surveys

In situ ground snow survey data used in this analysis were collected by the USACE St. Paul District. SWE measurements are collected by the St. Paul District each year in order to determine how much water equivalent is contained in the snowpack, primarily for spring flood risk assessment and reservoir management. All snow survey measurements were taken by sampling the snowpack in undisturbed areas (e.g., no snow drifting) that appeared to be representative of the surrounding area. To obtain each snow sample, a 3.81-cm diameter snow tube was driven vertically downward from the snow surface to the ground surface, using a rotating motion so that the saw teeth on the tube cut a core. A shovel was then placed at the bottom of the core to minimize sample loss, and the snow was emptied into a plastic bag and weighed (subtracting the weight of the bag). At each site, at least four snow samples were taken, each approximately 3–4 m apart, along with corresponding snow depth measurements obtained with a ruler (William Odell, USACE, personal communication). The four or more measurements were used to calculate SWE, then averaged to obtain a single mean value for the site on the given day. Snow density was calculated as average SWE divided by average snow depth.

Ice lenses, ground ice, and depth hoar are difficult to accurately sample using ground survey methods, especially with small-diameter snow tubes, and can lead to underestimates of SWE (Carroll, 2001). Additionally, these data are essentially point observations and may not be representative of large areas. However, ground SWE surveys are generally considered to be the most accurate observations of SWE because of the direct nature of the estimation method.

The USACE St. Paul District maintains two types of established ground snow survey sites. There are 24 "weekly" sites in the District, but only four are within the study area of this analysis (black polygonal symbols in Figure 1, right panel). SWE is measured at these sites on an approximately weekly basis from first snowfall to snow disappearance in the spring, with a total of 539 SWE observations available for the four sites during the operational period of AMSR-E (470 of which were also coincident with AMSR-E observations). "Annual" sites are sampled approximately once per year, often in late February, for years when there is a significant snowpack and risk of spring flooding (circles in Figure 1, right panel). There are 254 annual sites in the St. Paul District, 117 of which fall within the study area and were sampled during the operational period of AMSR-E (for a total of 760 observations, 702 of which were also coincident with AMSR-E observations). The USACE data were obtained from the St. Paul District website (http://www.mvp-wc.usace.army.mil/projects/) and via communication with the USACE St. Paul District.

3.3 | OWP airborne gamma radiation SWE surveys

Gamma radiation is naturally emitted from radioisotopes in soil, including potassium, uranium, and thorium. Water in any phase attenuates the gamma radiation emitted from the ground, which derives from approximately the top 20 cm of soil (Carroll & Schaake Jr, 1983). Attenuation can occur due to the presence of soil moisture, ground ice, standing water, snow, or ice lenses or liquid water in the snowpack and depends only on water mass (Carroll, 2001).

Research on the use of natural terrestrial gamma radiation to estimate SWE in the United States and Canada began in the late 1960s (Grasty, 1982; Peck et al., 1971), with an operational flight line network established by the NWS in 1980 (Peck et al., 1980), primarily in order to assist with flood forecasting. Currently, the NWS flight line network comprises over 2,400 flight lines covering parts of 29 states and seven Canadian provinces (Carroll, 2001; http://www.nohrsc.noaa.gov) and is maintained by the NOAA OWP. On average, each flight line is approximately 15–20 km long and 330 m wide, with an areal footprint of 5–7 km^2. Gamma radiation is measured using a detector housed in an aircraft that flies at an altitude of 150 m above the ground along a given flight line (Carroll, 2001). Gamma radiation counts are collected along the flight line, as well as the respective energy of each detected particle, and a weighted moisture estimate is calculated using the photopeaks of ^{40}K, ^{208}Tl, and for the total count across the measured spectrum (0.41–3.0 MeV; Carroll, 2001; Carroll & Schaake Jr, 1983). The counts are corrected to account for atmospheric radon, cosmic radiation, Compton scattering, background radiation from the aircraft and detection system, and attenuation due to the air mass between the ground and the detector (Carroll & Schaake Jr, 1983; Peck et al., 1971; Peck et al., 1980). Flight lines are typically measured once over bare soil in the fall, and later over snow-covered ground in the winter. The difference between the measurements allows for calculation of SWE, where the soil moisture is assumed to remain constant from the fall to winter measurements (Carroll, 2001; Carroll & Schaake Jr, 1983).

The OWP gamma radiation snow survey program provides SWE measurements over the Northern Great Plains, but operational restrictions limit observations to four or less times per flight line per year. Over 27,000 OWP gamma survey estimates are available from 1979 to present across the North America, with a total of 2,335 observations over 449 flight lines falling within the AMSR-E operational period and the study area of this analysis (of which 2,131 observations over 423 flight lines were coincident with AMSR-E SWE observations). The airborne gamma radiation SWE data were obtained from the OWP (NOHRSC) website (http://www.nohrsc.noaa.gov/snowsurvey/) (National Operational Hydrologic Remote Sensing Center, 2004). The flight lines are shown as black lines in Figure 1 (left panel).

4 | METHODS

This analysis evaluates AMSR-E SWE data against the other two sets of SWE observations: (1) USACE ground survey SWE and (2) OWP airborne gamma radiation survey SWE. In the first analysis, the AMSR-E SWE were directly validated against the USACE snow survey SWE measurements. This analysis treats the USACE SWE data as point measurements. The USACE SWE data (both "weekly" and "annual" sites) are compared directly to the daily AMSR-E SWE value for the 25-km pixel that encompassed the given survey location.

Unfortunately, most pixels only contained a single snow survey location. Chang et al. (2005) indicated that more than 10 point estimates of snow depth within a 1° pixel are necessary to obtain an error of 50 mm between in situ and SSM/I satellite estimates. In order to roughly estimate the error inherent in the spatial representativeness of the snow surveys, an additional simulation analysis was conducted. For this simulation, the AMSR-E data were treated as perfect SWE measurements (i.e., no measurement or algorithm estimation error, although this is not realistically the case). Then normally distributed random error with a standard deviation of 25 mm (and mean of 0 mm) was added to the AMSR-E data (and SWE could not be less than zero), to simulate the effect of subpixel-scale heterogeneity on an otherwise perfect measurement. The AMSR-E SWE data plus error are analogous to point measurements of SWE. We used these simulated "point measurements," to estimate the amount of error due to the scale mismatch between in situ SWE measurements and satellite estimates (considering only small-scale heterogeneity in SWE). The value of 25 mm was an estimate obtained by applying the mean coefficient of variation for mid-latitude prairie from Figure 2 in Clark et al. (2011) to the mean of the AMSR-E data in our study. We found that a constant error value better represented the error pattern that we observed between USACE and AMSR-E SWE, compared to a constant coefficient of variation (which underestimated variability at low SWE, and overestimated variability at high SWE).

The OWP gamma survey SWE observations were also compared to AMSR-E SWE. The gamma flight lines frequently overlapped more than one AMSR-E pixel. In order to compare the OWP gamma SWE and AMSR-E SWE data, the area-weighted average AMSR-E SWE within the effective footprint of each flight line was calculated. For each OWP flight line, an effective polygonal measurement footprint was determined using a flat capped, rounded corner buffer around the given flight line, with a fixed radius of 165 m (i.e., diameter of 330 m; Carroll, 2001; see left panel of Figure 2). On any day when gamma measurements were collected, the AMSR-E SWE data within the given flight line footprint were averaged and weighted according to the area of the footprint contained within each AMSR-E pixel. If AMSR-E SWE data were not available for a portion of the flight line footprint, the weighted SWE value was calculated using the area of the footprint with available data. Flight lines with AMSR-E SWE data covering less than 50% of the footprint area were excluded from the analysis. A general flow chart for this procedure is shown in the right panel of Figure 2.

5 | RESULTS

The four weekly USACE snow survey sites provide information on snowpack properties in the study area. Figure 3 shows the mean evolution of snow properties in the study area over the course of the winter during the study period (June 18, 2002, until October 4, 2011).

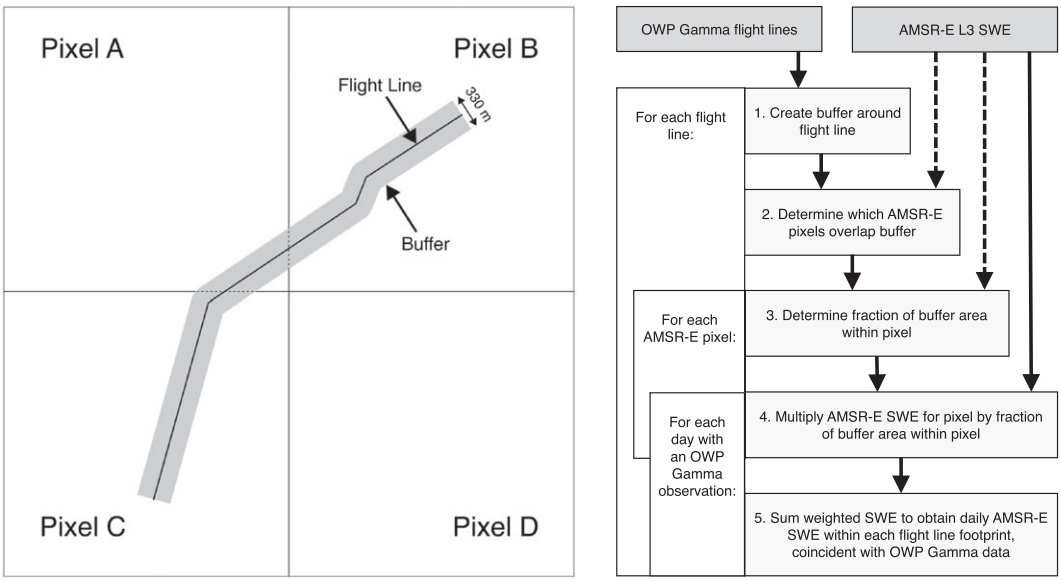

FIGURE 2 Schematic diagram showing how Advanced Microwave Scanning Radiometer for the Earth Observing System (AMSR-E) snow water equivalent (SWE) data were processed for comparison to OWP gamma SWE. The left panel shows how individual Office of Water Prediction (OWP) flight lines (black line) could overlap multiple AMSR-E pixels (note: pixels not to scale), and how a buffer (grey area) was used around the flight line to represent the effective sampling area of the method. The right panel details the steps used to obtain area-weighted AMSR-E SWE values to compare to each OWP gamma observation. The area of the flight line buffer that fell within each pixel was used to weight the AMSR-E SWE value of that pixel during averaging (i.e., Step 4)

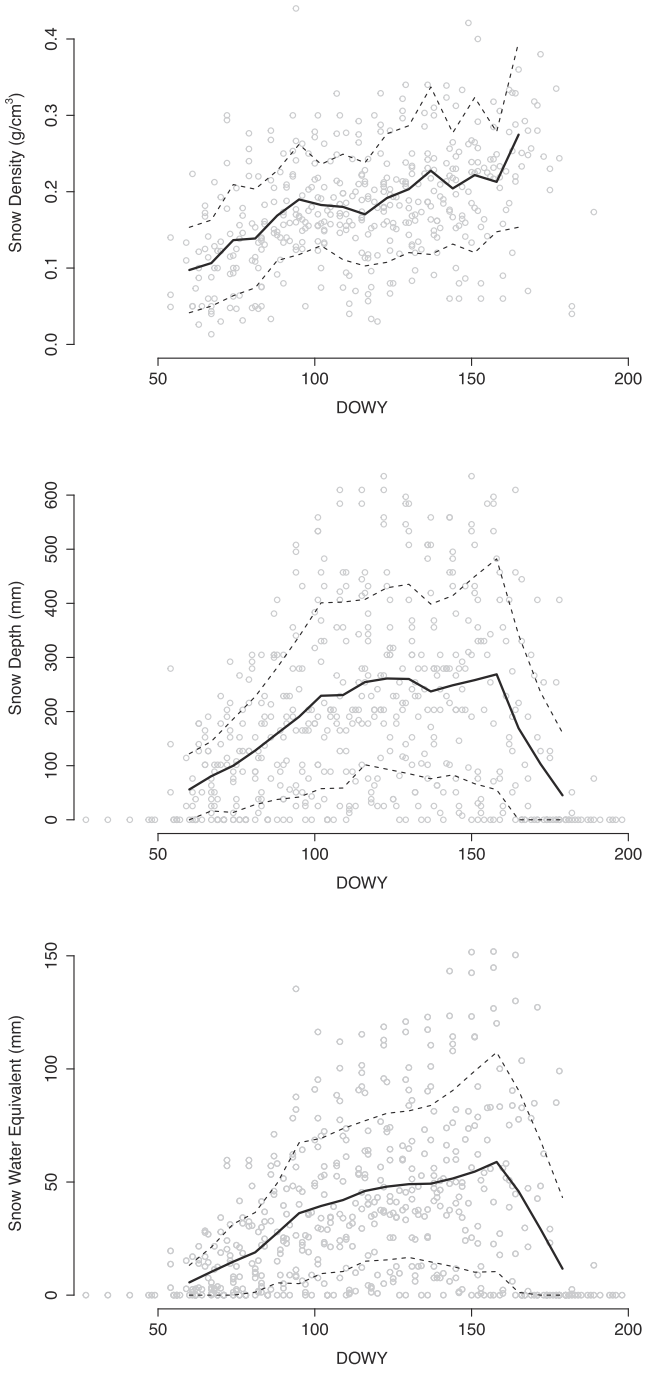

FIGURE 3 Mean annual temporal evolution of snow properties as determined from the U.S. Army Corps of Engineers weekly survey sites within the study area and during the time period of Advanced Microwave Scanning Radiometer for the Earth Observing System. The top panel shows snow density, the middle panel shows snow depth, and the bottom panel shows snow water equivalent. Measurements from all sites and years are plotted as a function of day of water year (DOWY; grey circles). The solid black line is the mean, calculated for weekly bins, and the dotted lines show the mean plus or minus one standard deviation

The snow density increases steadily throughout the winter, from the first snowfall until snowmelt, due to compaction and snowpack metamorphism. The snow depth also increases fairly linearly from early December (day of water year 60 [DOWY 60]) until early February (DOWY 124) before levelling out and remaining fairly constant until approximately the second week in March (DOWY 160). At this point, the snow depth rapidly declines as the snowpack melts, with complete snowpack disappearance typically by the beginning of April (DOWY 184). The SWE follows a similar pattern to snow depth, except that it monotonically increases until approximately DOWY 160, after which it rapidly declines, consistent with the snow depth. Unlike the snow depth, the SWE increase from early February through early March. Increase in the SWE (i.e., snowfall) during this midwinter period is balanced by increasing snow density, leading to a fairly constant snow depth. The snowpack typically lasts approximately 17 weeks, but there is significant interannual variability.

5.1 | AMSR-E versus USACE SWE

The AMSR-E SWE generally captures SWE timing and evolution across years at the USACE survey sites (Figure 4). The USACE and AMSR-E SWE data agree fairly well, although some years exhibit bias (e.g., Baldhill in 2010, Lac Qui Parle in 2008). The initial snow accumulation phase from the passive microwave SWE appears to track quite well with the USACE in situ surveys. The abrupt end of season snow melt captured by the microwave is also generally well supported by the USACE in situ surveys. The daily microwave SWE observations reflect the overall seasonal trends of the weekly USACE in situ surveys, but with greater scatter. In general, the AMSR-E SWE magnitude at these same locations is lower than the USACE SWE throughout the winter (mean difference of 7 mm). However, there is considerable day-to-day and year-to-year variability. This suggests that even within a relatively small region, large differences between data sources may exist, possibly due to differences in scale or local landscape effects on snow distribution.

Figure 5 shows scatter plots of USACE snow survey SWE versus the AMSR-E SWE for the pixel that contains each given USACE site. Despite the generally good correspondence in the SWE time series, there is a fair amount of scatter. The upper bound on the USACE snow survey values is about 150 mm, whereas AMSR-E has some higher SWE values. For lower SWE conditions, AMSR-E shows numerous values of 0 mm despite a wide range of USACE values.

The summary statistics in Table 1 indicate that the bias (i.e., mean signed difference, MSD) between the USACE and AMSR-E SWE is small, signifying good agreement between the estimates when the data are considered as a whole. Additionally, the satellite variability is similar to that from the point samples. However, there is a large root mean squared difference (RMSD) between AMSR-E and USACE SWE estimates (34.7 mm overall). The mean absolute difference (MAD) values are 10 mm lower than the RMSD values, reflecting the greater observed bias for higher SWE values. Overall, the AMSR-E SWE agrees better with the weekly USACE SWE values than those from the annual sites. However, the weekly and annual sites show no difference in agreement with AMSR-E SWE over an SWE range of approximately 30–110 mm. The annual USACE SWE data are often collected when the snowpack is at its deepest, so the AMSR-E versus weekly site statistics benefit from lower SWE values other parts of the winter, which better agree with AMSR-E observations. Much of the difference between the microwave and in situ SWE can likely be attributed to the large-scale disparity between the two measurements and spatial

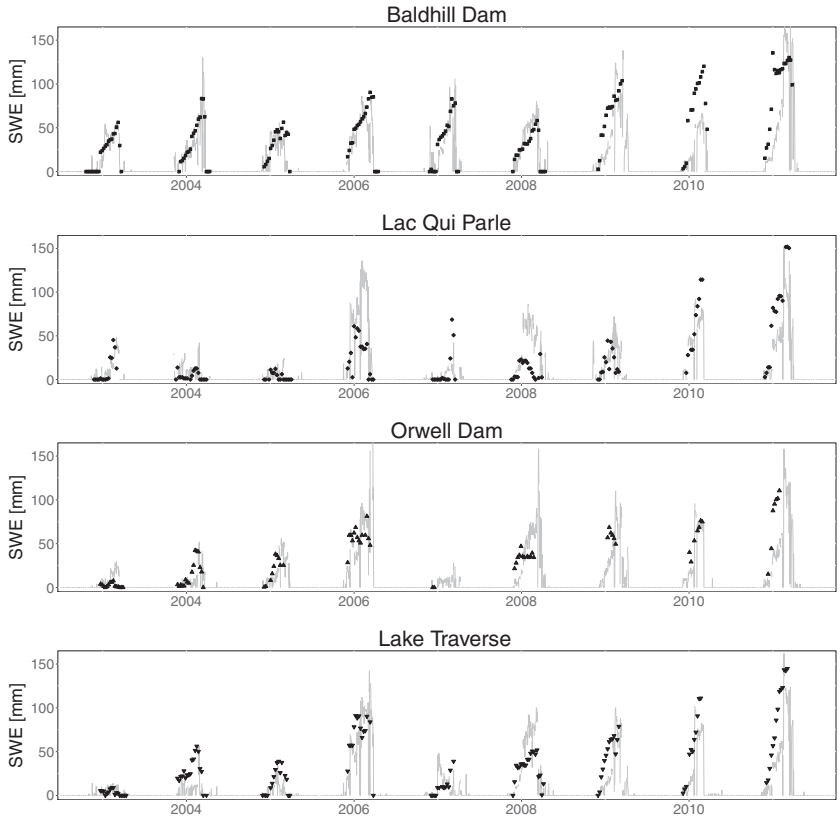

FIGURE 4 Time series plots of the U.S. Army Corps of Engineers weekly survey sites compared to the Advanced Microwave Scanning Radiometer for the Earth Observing System snow water equivalent (SWE) value for the respective pixel that contains each site. U.S. Army Corps of Engineers data are plotted as black points, whereas the Advanced Microwave Scanning Radiometer for the Earth Observing System data are shown in grey lines. From top to bottom, the plots show the SWE values at the Baldhill Dam, Lac Qui Parle, Orwell Dam, and Lake Traverse sites

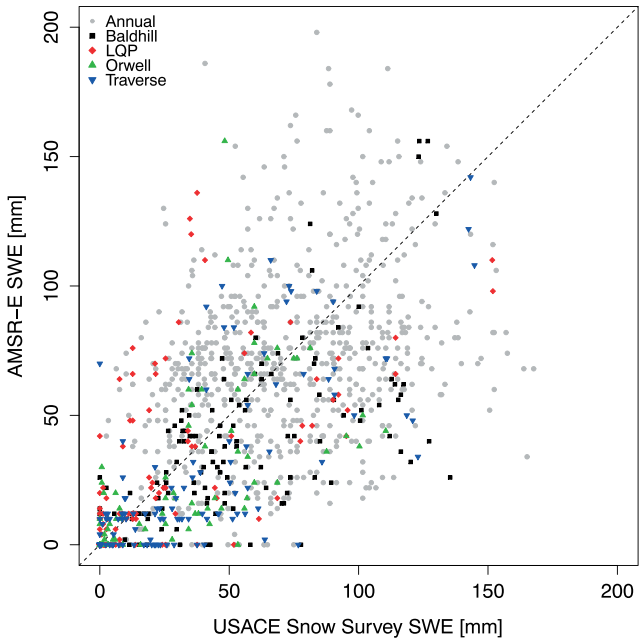

FIGURE 5 Plot of U.S. Army Corps of Engineers (USACE) ground snow survey snow water equivalent (SWE) versus Advanced Microwave Scanning Radiometer for the Earth Observing System (AMSR-E) SWE for the pixel that contains the given survey site. Annual survey sites are plotted in grey, whereas the four weekly survey sites are each plotted with a different colour and symbol. The black dotted line indicates 1:1 agreement

variability in snow cover, because the USACE data are essentially point data, whereas the AMSR-E footprint is 625 km^2. Although there is not adequate USACE sampling to quantify the effect of that spatial heterogeneity within a single AMSR-E pixel footprint, previous studies clearly indicate large within-footprint variability (e.g., Clark et al., 2011). In an attempt to quantify this heterogeneity error, we conducted a simulation experiment to quantify the effect of small-scale heterogeneity on an otherwise perfect measurement. When a normally distributed random error with a standard deviation of 25 mm was added to the AMSR-E data, the resulting RMSD between unaltered AMSR-E SWE and AMSR-E SWE with added random error was 23 mm. This indicates that approximately 44% of the mean squared difference (MSD) is potentially due to subpixel-scale spatial heterogeneity, rather than measurement error in either data source. However, the method used by the USACE, that is, to collect four SWE samples at each site and report the mean, may somewhat reduce the contribution of micro-scale heterogeneity to the observed RMSD. An analogous simulation analysis, where four replicates with random error were averaged together then compared back to the AMSR-E data, indicated RMSD values of 12 mm due to subgrid-scale variability (which accounts for 12% of the MSD). Subgrid-scale spatial variability of SWE is further discussed in Section 6.2.

5.2 | AMSR-E versus OWP gamma SWE

Figure 6 shows a scatter plot of OWP gamma survey SWE for each OWP flight line versus the weighted average AMSR-E SWE within the given flight line. The AMSR-E SWE appears to have a greater range over the winter than the gamma SWE. It is expected that SWE will generally increase throughout the winter, before melting in the spring (e.g., Figures 3 and 4). If the AMSR-E and gamma estimates detected this behaviour equally, then the points would generally increase along the 1:1 line as a function of DOWY. However, in Figure 6, the AMSR-E SWE appears to increase more as a function of DOWY than the OWP

TABLE 1 Agreement between USACE and AMSR-E SWE

Time period	n	$\overline{SWE_A}$ (mm)	$\overline{SWE_U}$ (mm)	s_A (mm)	s_U (mm)	*MSD* (mm)	*MAD* (mm)	*RMSD* (mm)	a	b (mm)	R^2	τ
All	1172	53.3	57.1	39.1	38.0	−3.8	26.2	34.7	0.62	18.2	0.36	0.46
Annual	702	69.8	71.6	34.2	32.3	−1.7	31.3	38.6	0.34	45.0	0.11	0.23
Weekly	470	28.7	35.5	32.4	35.6	−6.8	18.7	27.9	0.62	6.6	0.47	0.58
Baldhill	151	33.1	45.7	31.9	37.3	−12.7	19.4	29.2	0.62	4.9	0.51	0.59
LQP	122	24.8	22.6	32.4	33.0	2.2	16.7	27.4	0.64	10.4	0.42	0.59
Orwell	76	28	33.6	30.8	29.5	−5.6	18.8	27.4	0.63	7.0	0.36	0.54
Traverse	121	27.5	36.8	33.6	35.7	−9.3	19.5	27.1	0.69	2.2	0.53	0.56

Note. USACE = U.S. Army Corps of Engineers; AMSR-E = Advanced Microwave Scanning Radiometer for the Earth Observing System; SWE = snow water equivalent; *n* = number of observations; $\overline{SWE_A}$ = mean AMSR-E SWE; $\overline{SWE_U}$ = mean USACE SWE; s_A = standard deviation of AMSR-E SWE; s_U = standard deviation of USACE SWE; *MSD* = mean signed difference between AMSR-E and USACE SWE; *MAD* = mean absolute difference; *RMSD* = root mean squared difference; *a* = slope of linear regression between AMSR-E and USACE SWE; *b* = y-intercept of linear regression; R^2 = coefficient of determination; τ = Kendall's rank correlation coefficient.

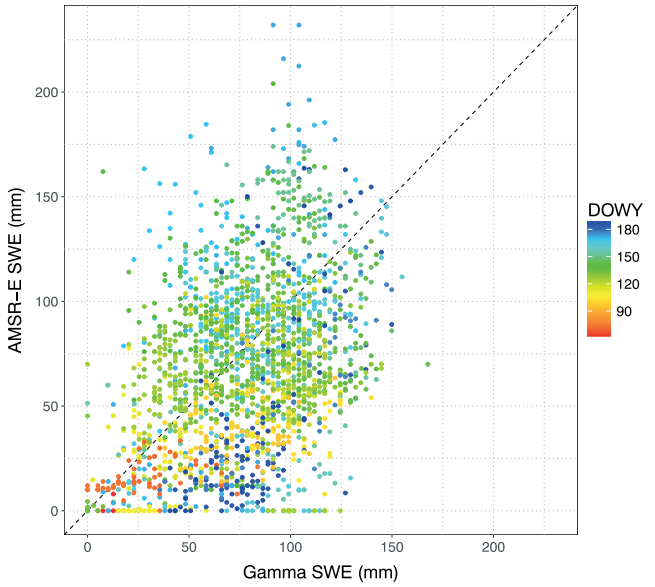

FIGURE 6 Plots of Office of Water Prediction gamma snow water equivalent (SWE) versus weighted-average Advanced Microwave Scanning Radiometer for the Earth Observing System (AMSR-E) SWE within the given flight line footprint. The points are coloured by day of water year (DOWY; i.e., day of year starting on October 1—Day 93 is January 1). The dotted black line "indicates 1:1 agreement

gamma SWE, as the DOWY colouring moves generally upward along the AMSR-E axis. This could potentially indicate that the AMSR-E SWE algorithm does not adjust enough to the changing snow grain size and density as the snowpack metamorphoses over the course of the winter. A cyclical pattern is also evident in Figure 6, the SWE increases slowly from December to February but decreases quickly in March (blue points), presumably due to the spring melt. There seems to be some hysteresis in this pattern, as most of the dark blue points fall at the right-hand edge of the point cloud, indicating that the OWP gamma estimate is higher than the AMSR-E estimate as the snowpack decreases in late winter to spring.

There is also a large amount of the data below the 1:1 line, indicating that the AMSR-E estimates were often low compared to the OWP gamma estimates. This pattern could potentially stem from a handful of factors. First, the snowpack or ground surface could be wet, which depresses the AMSR-E SWE estimate but does not affect the OWP estimate (Carroll & Carroll, 1989; Stiles & Ulaby, 1980). Kelly and Chang (2003) noted a similar hysteresis pattern between in situ snow depth and brightness temperature difference between 19 and 37 GHz brightness temperatures (vertical polarization), which the authors attributed to liquid water in the snowpack. Second, the fall soil moisture estimate necessary to calculate SWE using the OWP gamma method could be too low, resulting in an increased SWE estimate. Third, the OWP gamma measurement could detect snowmelt-derived liquid water that has percolated into the upper soil during the winter (i.e., increased soil moisture compared to the fall soil moisture estimate), which could lead to an overestimation of SWE (Peck et al., 1980), or even a non-zero SWE value when there is no snowpack. However, it is difficult to determine which factor is most responsible for disagreement in SWE due to observation limitations. MODIS imagery could help to determine snow cover versus bare ground conditions, but clouds often obscure view of the ground and melting can occur quickly. Independent observations of snow wetness in this region are non-existent and few shallow soil moisture measurements exist.

Figure 7 shows the same data from Figure 6, but separated by winter. In this context, it is apparent that the gamma estimates are clustered in time (i.e., by "campaign"). Each campaign shows consistent behaviour, but the agreement between the AMSR-E and OWP gamma SWE estimates varies greatly, with some campaigns falling approximately along the 1:1 line, and some deviating far from it (e.g., yellow and cyan points in winter 2006–2007). This again highlights the importance of snow and soil moisture conditions on the agreement between the SWE estimates, because the effect of wet snow on AMSR-E SWE or the effect of an inaccurate soil moisture estimate on OWP gamma SWE could each lead to large differences in agreement across different gamma campaigns. Variability in atmospheric conditions or radon concentrations (Peck et al., 1980) might also partly explain this clustering behaviour.

Table 2 presents agreement statistics between the AMSR-E and gamma SWE estimates, both overall and by month. Overall, the agreement is weaker than in the USACE snow survey comparison (Table 1). There is a large bias in all months except February and March. The MAD and RMSD are considerably higher for the gamma comparison than for the USACE snow surveys (Table 1) despite the larger areal footprint of the gamma observations.

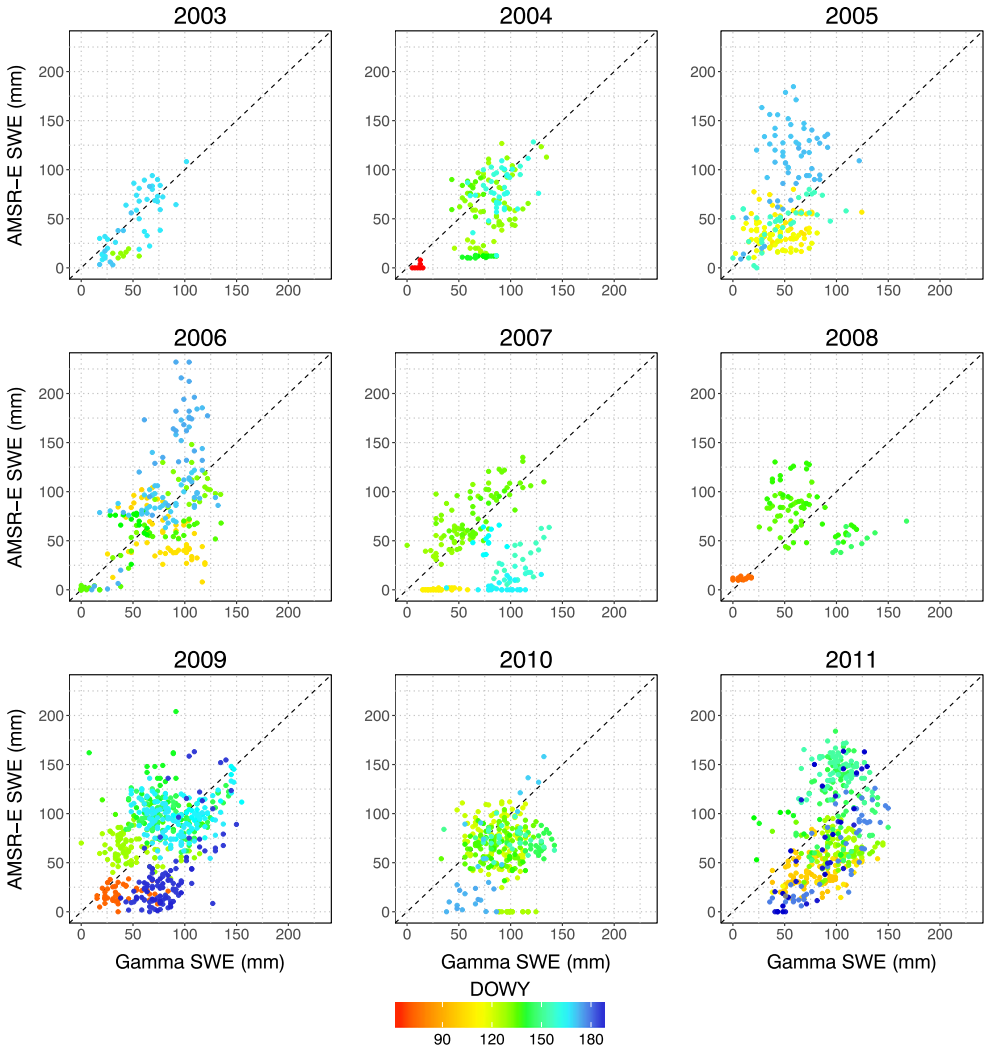

FIGURE 7 Same as Figure 6, but plotted individually by water year (i.e., water year 2003 encompasses winter 2002–2003). Office of Water Prediction observations are often collected for multiple flight lines in a short time period (i.e., grouped into "campaigns" that last only a few days). SWE = snow water equivalent; AMSR-E = Advanced Microwave Scanning Radiometer for the Earth Observing System

TABLE 2 Agreement between OWP gamma and AMSR-E SWE

Time period	n	$\overline{SWE}_A$ (mm)	$\overline{SWE}_G$(mm)	s_A (mm)	s_G (mm)	*MSD* (mm)	*MAD* (mm)	*RMSD* (mm)	a	b (mm)	R^2	τ
All	2131	68.5	78.0	40.9	31.4	−9.5	34.0	42.7	0.47	32.0	0.13	0.24
Dec.	65	14.9	33.3	8.5	45.3	−18.5	20.6	48.3	0.02	14.0	0.02	0.38
Jan.	386	46.9	70.6	26.7	28.3	−23.6	31.8	38.1	0.39	19.6	0.17	0.29
Feb	940	77.7	81.2	36.0	30.5	−3.5	32.8	40.3	0.33	51.1	0.08	0.16
Mar.	592	79.8	81.4	44.7	29.7	−1.6	35.6	46.3	0.42	46.0	0.08	0.16
Apr.	147	45.1	83.2	44.1	24.6	−38.1	46.3	50.6	1.19	−53.6	0.44	0.47
May	1	16	50.8	-	-	−34.8	34.8	34.8	-	-	-	-

Note. Columns are identical to Table I, except that OWP gamma SWE ("G") has replaced USACE SWE. OWP = Office of Water Prediction; SWE = snow water equivalent; USACE = U.S. Army Corps of Engineers.

For most OWP flight lines, fall soil moisture is measured using the aircraft gamma instrument, but for others, it is derived from interpolation between other measured flight lines, or estimated subjectively from based on qualitative information or ground measurements. The best agreement occurs when the fall soil moisture is measured (*MSD* = −2.5 mm, *MAD* = 31.9 mm, and *RMSD* = 41.3 mm), rather than interpolated from estimates (*MSD* = −16.4 mm, *MAD* = 35.2 mm, and *RMSD* = 45.8 mm). However, good agreement also occurs when the fall soil moisture is estimated subjectively or based on supplemental data (*MSD* = −9.9 mm, *MAD* = 28.0 mm, and *RMSD* = 35.9 mm). These results underscore that there is variability in soil moisture between flight lines, and measuring fall soil moisture immediately before the winter freeze-up would help to obtain accurate SWE estimates, but often logistical and operational realities do not make this possible.

6 | DISCUSSION

6.1 | Comparison to other studies

Comparison between individual USACE ground survey SWE estimates and AMSR-E SWE from the encompassing pixel indicated a mean bias (i.e., MSD) and RMSD of −3.8 and 34.7 mm, respectively. These values are much higher than an early validation study between OWP gamma and ground SWE estimates in the Upper Midwest (*RMSE* = 8.8 mm, bias = +5.4 mm; Carroll & Schaake Jr, 1983). However, it is important to note that the validation study involved exhaustive sampling of SWE and snow depth, as well as vegetation water content measurements, so agreement between single ground sites and OWP gamma estimates might be less ideal (Barry Goodison, personal communication).

The agreement statistics from this study are similar to those found in other analyses. Byun and Choi (2014) compared AMSR-E SWE estimates to SWE derived from in situ snow depth measurements multiplied by an assumed snow density of 0.275 g/cm^3 (or a dynamic density from Sturm et al., 2010). The authors found RMSE values ranging between 4.03 and 57.56 mm for the months of December to February for four sites (static density) and mean absolute error (MAE) values from +1.08 (+0.60) to +35.18 (+37.75) mm (static and dynamic). These values bracket the statistics found in this study, whereas R^2 values are similar. Three of the four sites showed better agreement than any of the USACE sites or monthly OWP gamma SWE in this study, but these three sites had much lower in situ SWE (maximum of 50–80 mm) than the sites from this study (maximum of 165 mm). Tong and Velicogna (2010) compared AMSR-E SWE to SWE derived from in situ snow depth measurements multiplied by a regionally and seasonally varying snow density for four winter seasons at six sites (Brown, Derksen, & Wang, 2007). The authors found monthly MAE values ranging between approximately 12 and 50 mm for December through March. The MAE values from this study using USACE SWE fall in the low to middle portion of this range, whereas OWP gamma SWE MAE falls in the upper portion of the range. Yang et al. (2015) compared AMSR-E SWE to SWE derived from in situ snow depth measurements across the Tibetan Plateau. They found an overall RMSE of 38.1 mm, with values of 36.6 and 25.6 mm for grassland and barren areas, respectively. These values match closely with the RMSD found in this study between USACE and AMSR-E SWE.

Additionally, Mote et al. (2003) found biases between monthly mean in situ and 1° SSM/I SWE of −20 to +7 mm at five stations in the Northern Great Plains, using the Meteorological Service of Canada satellite algorithm. The authors compared estimates at daily temporal scale as well but did not report agreement statistics. Tekeli (2008) found relative agreement of −78% to +218%, and an R^2 of 0.10, between 48 in situ snow courses and AMSR-E estimates in eastern Turkey. Derksen, Walker, and Goodison (2003) found seasonal mean bias errors between 5-day in situ and passive microwave SWE (Scanning Multichannel Microwave Radiometer (SMMR) and SSM/I, Meteorological Service of Canada algorithm) of 15 mm or less for 13 stations in western Canada over 18 winters. Each of these studies highlighted the tendency of satellite microwave SWE to underestimate in situ SWE in early winter and overestimate in late winter. The authors noted that mid-winter melt events followed by snowpack refreeze led to overestimation, presumably due to increased snow density (and grain size). These studies also discussed the spatial scale difference between in situ and SSM/I SWE, as well as spatial variability at point scales (for which Schmidlin, Wilks, McKay, and Cember, 1995, found a coefficient of variation of 0.125, resulting in SWE deviations of up to 25% from the overall mean SWE for single point measurements).

The mean difference between AMSR-E and OWP gamma SWE in this study is −9.5 mm, and the RMSD is 42.7 mm. In the supposed "best case scenario" (i.e., where the soil moisture for the OWP gamma SWE estimates are from fall airborne gamma measurements), the mean difference is low (−2.5 mm) but the RMSD is still higher than the baseline AMSR-E versus USACE snow survey comparison (41.3 vs. 34.7 mm, respectively). Although 12–44% of the AMSR-E versus USACE comparison error can likely be attributed to point-scale heterogeneity, the spatial sampling error between AMSR-E and OWP gamma SWE is likely much smaller, due to the larger areal footprint of the gamma estimates (5–7 km^2). This suggests that there are errors present in the OWP data that are not shared by the USACE data and that outweigh the reduction in spatial sampling error gained from the USACE to OWP scale. It is likely that a large portion of the error between AMSR-E and OWP gamma SWE is due to the soil moisture assumptions that underlie the gamma estimates, which attempt to compensate for the greater observation depth of the gamma technique.

6.2 | Spatial variability in SWE

A portion of the difference between the AMSR-E and USACE SWE estimates can surely be attributed to the spatial variability of SWE, because USACE SWE is estimated at a much smaller scale than the 25-km resolution of AMSR-E. Chang et al. (2005) noted that considerable variability in snow depth exists within the spatial scale of satellite pixels in the Northern Great Plains and indicated that 10 measurements were needed within a 1° pixel in order to obtain an accuracy of 5 cm between SSM/I satellite and ground snow depth estimates. Dong et al. (2005) compared SMMR-derived 0.5° SWE to SWE derived from in situ snow depth measurements across Canada and found that SMMR pixels with five or more ground stations were generally unbiased with a median RMSE of 20 mm or less throughout each month of the winter, after screening for water body proximity, high air temperature, and high SWE values. The authors also found the lowest errors in the prairie snow class (from Sturm, Holmgren, & Liston, 1995), which is the dominant snow class of the study area for this analysis. However, the spatial density of in situ SWE measurement sites in the region of this study is not sufficient to similarly characterize SWE variability within individual 25-km resolution AMSR-E pixels. Chang and Rango (2000), using an equation from Snedecor and Cochran (1967), indicated that there is 95% confidence that the true mean of a pixel is within ±40 mm of the observed mean at a point, if the point SWE standard deviation is 20 mm and there is only one measurement point within a given pixel.

Most studies of SWE spatial variability using ground measurements have taken place at much smaller scales, up to 1 km^2 (Clark et al., 2011), due to the cost and effort required to conduct field surveys at larger scales. Notably, Watson, Anderson, Newman, Alexander, and

Garrott (2006) found that random SWE variation was common at small spatial scales (i.e., <10 m), but decreased to effectively zero at distances of 100 to 1,000 m. This supports the USACE technique of gathering multiple SWE samples in a small area and averaging to provide a single SWE estimate, as this method should mitigate point-scale random SWE variability. Vander Jagt, Durand, Margulis, Kim, and Molotch (2013) found that passive microwave brightness temperatures are sensitive to the mean snow depth within the sensor footprint, despite heterogeneity in snow properties, up to a scale of 1 km^2. So, as long as SWE measurement sites are altogether representative of the mean SWE within the pixel, there should be agreement between the ground and remote estimates. Meromy, Molotch, Link, Fassnacht, and Rice (2013) examined snow stations in the Western United States and found that over 50% of ground-based SWE measurement stations were within 10% of the mean SWE magnitude of the surrounding 1 km^2 (found using field surveys).

Multiple studies have found that SWE magnitude is related to physical properties of the land surface (such as elevation, slope, aspect, and vegetation type; Clark et al., 2011), which can partly explain SWE variability at large scales. Thus, landscapes with fewer changes in physical characteristics will presumably have lower SWE variability at large scales. This is encouraging for the Northern Great Plains, because topographic relief and vegetation cover are low, so there should not be much change in snow type. However, drifting of snow is significant in the region (Cork & Loijens, 1980; Pomeroy, Gray, & Landine, 1993), and the presence of vegetation, raised roads, fences, and shelter belts (which catch wind-blown snow) could create systematic SWE patterns that might not be captured by the USACE data.

Airborne gamma radiation estimates obtain SWE estimates over larger areas than the USACE sites and thus will average over some systematic SWE patterns. However, SWE spatial variability could similarly affect the AMSR-E versus OWP gamma comparison. The OWP flight lines often comprise parts of multiple AMSR-E pixels (Figure 1), so in order to compare the two SWE data sources, the weighted mean AMSR-E SWE was found for the footprint of the given flight line. However, it is possible that the portion of the AMSR-E pixels within the flight line footprint is not representative of the AMSR-E pixel as a whole, thus introducing error into the comparison. It is unclear how to best quantify this error given the currently available SWE data, because the airborne gamma data, unlike the USACE SWE sites, are not neatly contained within one AMSR-E pixel. Coordinated field campaigns would enable better characterization of SWE spatial variability within the satellite footprints in the Northern Great Plains, both at the point and flight line scales.

7 | CONCLUSION

Although SWE in the Northern Great Plains area has been studied in the past, especially during the development of passive microwave and gamma radiation methods in the 1970s and 1980s, greater spatial coverage of accurate SWE data is needed for operational flood forecasting. The OWP gamma radiation snow survey program provides a vital data set of SWE measurements over this area, but each flight line is only measured a maximum of four times per winter (and usually only once or twice). High-quality in situ measurements of SWE are sparse, and only a handful of sites collect measurements on a daily basis in the Northern Great Plains. For this reason, accurate determination of SWE for operational flood forecasting purposes remains difficult. Satellite passive microwave observations have the potential to fill this knowledge gap for large scales and daily frequency.

AMSR-E passive microwave and USACE snow survey SWE observations in the Northern Great Plains agree with a bias and RMSD of −3.8 and 34.7 mm, respectively. A simulation analysis suggests that small-scale variability in SWE accounts for 12–44% of the observed error between AMSR-E and USACE SWE observations, depending on whether or not USACE observations are considered a single point measurement or the mean of four points. Given this, we estimate the maximum achievable RMSD between in situ and operational satellite SWE is approximately 26–33 mm in the Northern Great Plains. By collecting five in situ measurements within a single satellite pixel, the error due to small-scale variability can be decreased by approximately 80% (as compared to only one measurement per pixel), whereas collecting 10 in situ measurements leads to an additional 10% decrease in error.

AMSR-E SWE shows poorer agreement with OWP gamma SWE than with USACE ground survey SWE, despite the much larger measurement footprint of the former observation method. For this reason, gamma SWE estimates should be used in concert with other SWE measurements, such as in situ or satellite measurements, rather than in isolation. The greater penetration depth of the gamma radiation method provides slightly different information than either the passive microwave or manual sampling methods, which may provide useful hydrological context. However, SWE estimation from airborne gamma radiation measurements requires multiple assumptions (e.g., soil moisture content in the upper soil) that can result in significant errors, so it is important to accurately characterize the environmental conditions that contribute to these error sources.

In summary, our analyses indicate that satellite estimates agree with in situ and airborne gamma SWE estimates with mean differences of less than 10 mm and RMSDs of approximately 40 mm or less, despite the large disparity in spatial scale of the observations. However, more study and algorithm development is needed in order to better identify and account for changes in snow morphology and exclude satellite observations affected by the presence of liquid water (and potentially dense cloud cover). These uncertainties highlight the need for coordinated campaigns in the region, in order to address issues of scaling between different observations and better characterize snow morphology at large scales. Additionally, any future satellite campaigns (e.g., NASA SNOWEx in 2019–2021) to measure SWE will require validation at large scales (i.e., close to 25-km resolution), which will ideally entail continuous SWE measurement at denser resolution than is currently available. Satellite SWE missions could draw from the experience of the soil moisture community in order to establish such validation sites.

ACKNOWLEDGMENTS

The authors gratefully acknowledge support from NASA Applied Sciences Grant NNX15AC47G. The AMSR-E SWE data used in this research are freely available from the NASA National Snow and Ice Data Center (https://nsidc.org/data/ae_dysno), and the OWP airborne

gamma radiation survey SWE data are freely available from the NOHRSC website (http://www.nohrsc.noaa.gov/snowsurvey/). Thank you to Elizabeth Nelsen, Farley Haase, and William Odell of the USACE St. Paul District for providing the ground snow survey SWE data and information about the data collection and sampling methods. Thanks to Pedro Restrepo, Mike DeWeese, and Brian Connelly of the NOAA NCRFC for their input on the use of SWE data in operational flood forecasting. Additional thanks to Ronny Schroeder (UNH) for his insights about passive microwave satellite observations, and to Marina Reilly-Collette (USACE CRREL) for her suggestions about how best to compare the satellite and airborne gamma SWE data.

ORCID

Samuel E. Tuttle http://orcid.org/0000-0003-0154-6913
Jennifer M. Jacobs http://orcid.org/0000-0003-3824-6439

REFERENCES

Berghuijs, W. R., Woods, R. A., Hutton, C. J., & Sivapalan, M. (2016). Dominant flood generating mechanisms across the United States. *Geophysical Research Letters*, *43*(9), 4382–4390.

Brown, R., Derksen, C., & Wang, L. (2007). Assessment of spring snow cover duration variability over northern Canada from satellite datasets. *Remote Sensing of Environment*, *111*(2), 367–381.

Byun, K., & Choi, M. (2014). Uncertainty of snow water equivalent retrieved from AMSR-E brightness temperature in northeast Asia. *Hydrological Processes*, *28*(7), 3173–3184.

Carroll, S. S., & Carroll, T. R. (1989). Effect of uneven snow cover on airborne snow water equivalent estimates obtained by measuring terrestrial gamma radiation. *Water Resources Research*, *25*(7), 1505–1510.

Carroll, T. R. (2001). *Airborne gamma radiation snow survey program: A User's GUIDE, version 5.0*. (p. 14). Chanhassen: National Operational Hydrologic Remote Sensing Center (NOHRSC).

Carroll, T. R., & Schaake, J. C. Jr (1983, September). Airborne snow water equivalent and soil moisture measurement using natural terrestrial gamma radiation. In 1983 Technical Symposium East (pp. 208-213). International Society for Optics and Photonics.

Chang, A. T. C., Foster, J. L., & Hall, D. K. (1987). Nimbus-7 SMMR derived global snow cover parameters. *Annals of Glaciology*, *9*, 39–44.

Chang, A. T. C., Foster, J. L., & Hall, D. K. (1996). Effects of forest on the snow parameters derived from microwave measurements during the BOREAS winter field campaign. *Hydrological Processes*, *10*(12), 1565–1574.

Chang, A. T. C., Foster, J. L., Hall, D. K., Rango, A., & Hartline, B. K. (1982). Snow water equivalent estimation by microwave radiometry. *Cold Regions Science and Technology*, *5*, 259–267.

Chang, A. T. C., Foster, J. L., Kelly, R. E. J., Josberger, E. G., Armstrong, R. L., & Mognard, N. M. (2005). Analysis of ground-measured and passive-microwave-derived snow depth variations in midwinter across the Northern Great Plains. *Journal of Hydrometeorology*, *6*(1), 20–33.

Chang, A. T. C., & Rango, A. (2000). *Algorithm theoretical basis document (ATBD) for the AMSR-E snow water equivalent algorithm, version 3.1*. Greenbelt, Maryland USA: NASA Goddard Space Flight Center.

Chang, T. C., Gloersen, P., Schmugge, T., Wilheit, T. T., & Zwally, H. J. (1976). Microwave emission from snow and glacier ice. *Journal of Glaciology*, *16*(74), 23–39.

Clark, M. P., Hendrikx, J., Slater, A. G., Kavetski, D., Anderson, B., Cullen, N. J., … Woods, R. A. (2011). Representing spatial variability of snow water equivalent in hydrologic and land-surface models: A review. *Water Resources Research*, *47*(7).

Cork, H. F., & Loijens, H. S. (1980). The effect of snow drifting on gamma snow survey results. *Journal of Hydrology*, *48*(1–2), 41–51.

Derksen, C., Walker, A., & Goodison, B. (2003). A comparison of 18 winter seasons of in situ and passive microwave-derived snow water equivalent estimates in Western Canada. *Remote Sensing of Environment*, *88*(3), 271–282.

Dong, J., Walker, J. P., & Houser, P. R. (2005). Factors affecting remotely sensed snow water equivalent uncertainty. *Remote Sensing of Environment*, *97*(1), 68–82.

Foster, J. L., Barton, J., Chang, A. T., & Hall, D. K. (2001). Snow crystal and land cover effects on the scattering of passive microwave radiation for algorithm development. In: Europto remote sensing 2001. International Society for Optics and Photonics, pp. 149–155.

Foster, J. L., Chang, A. T. C., & Hall, D. K. (1997). Comparison of snow mass estimates from a prototype passive microwave snow algorithm, a revised algorithm and a snow depth climatology. *Remote Sensing of Environment*, *62*(2), 132–142.

Foster, J. L., Rango, A., Hall, D. K., Chang, A. T. C., Allison, L. J., & Diesen, B. C. (1980). Snowpack monitoring in North America and Eurasia using passive microwave satellite data. *Remote Sensing of Environment*, *10*(4), 285–298.

Gan, T. Y., Kalinga, O., & Singh, P. (2009). Comparison of snow water equivalent retrieved from SSM/I passive microwave data using artificial neural network, projection pursuit and nonlinear regressions. *Remote Sensing of Environment*, *113*(5), 919–927.

Grasty, R. L. (1982). Direct snow-water equivalent measurement by airborne gamma-ray spectrometry. *Journal of Hydrology*, *55*(1–4), 213–235.

Hallikainen, M. T., Ulaby, F. T., & Abdelrazik, M. (1986). Dielectric properties of snow in the 3 to 37 GHz range. *IEEE Transactions on Antennas and Propagation*, *34*(11), 1329–1340.

Hancock, S., Baxter, R., Evans, J., & Huntley, B. (2013). Evaluating global snow water equivalent products for testing land surface models. *Remote Sensing of Environment*, *128*, 107–117.

Josberger, E. G., & Mognard, N. M. (2002). A passive microwave snow depth algorithm with a proxy for snow metamorphism. *Hydrological Processes*, *16*(8), 1557–1568.

Josberger, E. G., Mognard, N. M., Lind, B., Matthews, R., & Carroll, T. (1998). Snowpack water-equivalent estimates from satellite and aircraft remote-sensing measurements of the Red River basin, north-central USA. *Annals of Glaciology*, *26*, 119–124.

Kelly, R. (2009). The AMSR-E snow depth algorithm: Description and initial results. *Journal of the Remote Sensing Society of Japan*, *29*(1), 307–317.

Kelly, R. E., Chang, A. T., Tsang, L., & Foster, J. L. (2003). A prototype AMSR-E global snow area and snow depth algorithm. *IEEE Transactions on Geoscience and Remote Sensing*, *41*(2), 230–242.

Kelly, R. E. J., & Chang, A. T. C. (2003). Development of a passive microwave global snow depth retrieval algorithm for Special Sensor Microwave Imager (SSM/I) and Advanced Microwave Scanning Radiometer-EOS (AMSR-E) data. *Radio Science*, *38*(4), 8076. https://doi.org/10.1029/2002RS002648

Liston, G., & Sturm, M. (2014). A global snow-classification dataset for earth-system applications. Unpublished work.

Mätzler, C. (1987). Applications of the interaction of microwaves with the natural snow cover. *Remote Sensing Reviews*, *2*(2), 259–387.

Meromy, L., Molotch, N. P., Link, T. E., Fassnacht, S. R., & Rice, R. (2013). Subgrid variability of snow water equivalent at operational snow stations in the western USA. *Hydrological Processes*, *27*(17), 2383–2400.

Mognard, M., & Josberger, E. G. (2002). Northern Great Plains 1996/97 seasonal evolution of snowpack parameters from satellite passive-microwave measurements. *Annals of Glaciology*, *34*(1), 15–23.

Mote, T. L., Grundstein, A. J., Leathers, D. J., & Robinson, D. A. (2003). A comparison of modeled, remotely sensed, and measured snow water equivalent in the Northern Great Plains. *Water Resources Research*, *39*(8), 1209. https://doi.org/10.1029/2002WR001782

National Operational Hydrologic Remote Sensing Center (2004). Airborne gamma radiation snow survey data products. Digital media.

North American Land Change Monitoring System (NALCMS) (2010). North American land cover at 250 m spatial resolution. (2010). Produced by Natural Resources Canada/Canadian Center for Remote Sensing (NRCan/CCRS), United States Geological Survey (USGS); Insituto Nacional de Estadística y Geografía (INEGI), Comisión Nacional para el Conocimiento y Uso de la Biodiversidad (CONABIO) and Comisión Nacional Forestal (CONAFOR). http://www.cec.org/tools-and-resources/map-files/land-cover-2010

Peck, E. L., Bissell, V. C., Jones, E. B., & Burge, D. L. (1971). Evaluation of snow water equivalent by airborne measurement of passive terrestrial gamma radiation. *Water Resources Research*, *7*(5), 1151–1159.

Peck, E. L., Carroll, T. R., & VanDemark, S. C. (1980). Operational aerial snow surveying in the United States/Etude de neige aérienne effectuée aux Etats Unis. *Hydrological Sciences Journal*, *25*(1), 51–62.

Pielke, R. A. (1999). Who decides? Forecasts and responsibilities in the 1997 Red River flood. *Applied Behavioral Science Review*, *7*(2), 83–101.

Pomeroy, J. W., Gray, D. M., & Landine, P. G. (1993). The prairie blowing snow model: Characteristics, validation, operation. *Journal of Hydrology*, *144*(1–4), 165–192.

Rannie, W. (2016). The 1997 flood event in the Red River basin: Causes, assessment and damages. *Canadian Water Resources Journal*, *41*(1–2), 45–55.

Schmidlin, T. W., Wilks, D. S., McKay, M., & Cember, R. P. (1995). Automated quality control procedure for the "water equivalent of snow on the ground" measurement. *Journal of Applied Meteorology*, *34*(1), 143–151.

Singh, P. R., & Gan, T. Y. (2000). Retrieval of snow water equivalent using passive microwave brightness temperature data. *Remote Sensing of Environment*, *74*(2), 275–286.

Snedecor, G. W., & Cochran, W. G. (1967). *Statistical methods* (6th ed.). (p. 593). Ames, Iowa: Iowa University Press.

Stadnyk, T., Dow, K., Wazney, L., & Blais, E.-L. (2016). The 2011 flood event in the Red River basin: Causes, assessment and damages. *Canadian Water Resources Journal*, *41*(1–2), 65–73.

Stiles, W. H., & Ulaby, F. T. (1980). The active and passive microwave response to snow parameters: 1. Wetness. *Journal of Geophysical Research*, *85*(C2), 1037–1044.

Sturm, M., Holmgren, J., & Liston, G. E. (1995). A seasonal snow cover classification system for local to global applications. *Journal of Climate*, *8*(5), 1261–1283.

Sturm, M., Taras, B., Liston, G. E., Derksen, C., Jonas, T., & Lea, J. (2010). Estimating snow water equivalent using snow depth data and climate classes. *Journal of Hydrometeorology*, *11*(6), 1380–1394.

Tedesco, M., Kelly, R., Foster, J. L., & Chang, A. T. C. (2004). *AMSR-E/Aqua Daily L3 Global Snow Water Equivalent EASE-Grids, version 2. AE_DySno*. Boulder, Colorado USA: NASA National Snow and Ice Data Center Distributed Active Archive Center. doi: https://doi.org/10.5067/AMSR-E/AE_DYSNO.002

Tedesco, M., & Narvekar, P. S. (2010). Assessment of the NASA AMSR-E SWE product. *IEEE Journal of Selected Topics in Applied Earth Observations and Remote Sensing*, *3*(1), 141–159.

Tedesco, M., & Wang, J. R. (2006). Atmospheric correction of AMSR-E brightness temperatures for dry snow cover mapping. *IEEE Geoscience and Remote Sensing Letters*, *3*(3), 320–324.

Tekeli, A. E. (2008). Early findings in comparison of AMSR-E/Aqua L3 global snow water equivalent EASE-grids data with in situ observations for Eastern Turkey. *Hydrological Processes*, *22*(15), 2737–2747.

Todhunter, P. E. (2001). A hydroclimatological analysis of the Red River of the North snowmelt flood catastrophe of 1997. *Journal of the American Water Resources Association*, *37*(5), 1263–1278.

Tong, J., & Velicogna, I. (2010). A comparison of AMSR-E/Aqua snow products with in situ observations and MODIS snow cover products in the Mackenzie River basin, Canada. *Remote Sensing*, *2*(10), 2313–2322.

Tuttle, S. E., Cho, E., Restrepo, P. J., Jia, X., Vuyovich, C. M., Cosh, M. H., & Jacobs, J. M. (2017). Remote sensing of drivers of spring snowmelt flooding in the North Central U.S. In V. Lakshmi (Ed.), *Remote sensing of hydrological extremes* (pp. 21–45). Cham, Switzerland: Springer International Publishing.

Ulaby, F. T., & Stiles, W. H. (1980). The active and passive microwave response to snow parameters: 2. Water equivalent of dry snow. *Journal of Geophysical Research*, *85*(C2), 1045–1049.

Vander Jagt, B. J., Durand, M. T., Margulis, S. A., Kim, E. J., & Molotch, N. P. (2013). The effect of spatial variability on the sensitivity of passive microwave measurements to snow water equivalent. *Remote Sensing of Environment*, *136*, 163–179.

Vuyovich, C. M., Jacobs, J. M., & Daly, S. F. (2014). Comparison of passive microwave and modeled estimates of total watershed SWE in the continental United States. *Water Resources Research*, *50*(11), 9088–9102.

Walker, A. E., & Goodison, B. E. (1993). Discrimination of a wet snow cover using passive microwave satellite data. *Annals of Glaciology*, *17*(1), 307–311.

Wang, J. R., & Tedesco, M. (2007). Identification of atmospheric influences on the estimation of snow water equivalent from AMSR-E measurements. *Remote Sensing of Environment*, *111*(2–3), 398–408.

Watson, F. G., Anderson, T. N., Newman, W. B., Alexander, S. E., & Garrott, R. A. (2006). Optimal sampling schemes for estimating mean snow water equivalents in stratified heterogeneous landscapes. *Journal of Hydrology*, *328*(3), 432–452.

Wazney, L., & Clark, S. P. (2016). The 2009 flood event in the Red River basin: Causes, assessment and damages. *Canadian Water Resources Journal*, *41*(1–2), 56–64.

Willmott, C. J., & Matsuura, K. (2001, updated 2015). Terrestrial air temperature and precipitation: Monthly and annual time series (1950–1999), University of Delaware, Newark, DE, USA. http://climate.geog.udel.edu/~climate/html_pages/README.ghcn_ts2.html.

Yang, J., Jiang, L., Ménard, C. B., Luojus, K., Lemmetyinen, J., & Pulliainen, J. (2015). Evaluation of snow products over the Tibetan plateau. *Hydrological Processes*, *29*(15), 3247–3260.

How to cite this article: Tuttle SE, Jacobs JM, Vuyovich CM, Olheiser C, Cho E. Intercomparison of snow water equivalent observations in the Northern Great Plains. *Hydrological Processes*. 2018;32:817–829. https://doi.org/10.1002/hyp.11459